The Effects of Rare Earth Pr and Heat Treatment on the Wear Properties of AZ91 Alloy

Ning Li [1,2] and Hong Yan [1,*]

1   School of Mechanical Electrical Engineering, Nanchang University, Nanchang 330031, China; lining@nchu.edu.cn
2   School of Aviation Manufacturing Engineering, Nanchang Hangkong University, Nanchang 330069, China
*   Correspondence: hyan@ncu.edu.cn; Tel.: +86-791-8396-9633; Fax: +86-791-8396-9622

Abstract: This paper investigated the influences of Pr addition and heat treatment (T6) on the dry sliding wear behavior of AZ91 alloy. The wear rates and friction coefficients were measured by using a pin-on-disc tribometer under loads of 30, 60 and 90 N at dry sliding speeds of 100 rpm, over a sliding time of 15 min. The worn surfaces were examined using a scanning electron microscope and was analyzed with an energy dispersive spectrometer. The experimental results revealed that AZ91-1.0%Pr magnesium alloy exhibited lower wear rate and friction coefficient than the other investigated alloys. As the applied load increased, the wear rate and friction coefficient increased. Compared with the as-cast AZ91-1.0%Pr magnesium alloy, the hardness and wear resistance of the alloy after solution treatment were reduced, and through the subsequent aging, the hardness and wear resistance of the alloy were improved and the hardness was 101.1 HB (compared to as-cast AZ91 magnesium alloy, it increased by 45%). The AZ91-1.0%Pr with T6 magnesium alloy exhibited best wear resistance. Abrasion was dominant at load of 30 N, delamination was dominant at load of 60 N and plastic deformation was dominant at load of 90 N. Oxidation was observed at all loads.

Keywords: AZ91 alloy; Pr; heat treatment; wear resistance

1. Introduction

AZ91 magnesium alloy is excellent and the most widely used of die-casting magnesium alloys, due to its high strength-to-weight ratio, suitable corrosion resistance and mechanical properties for room temperature application [1–3]. AZ91 Magnesium alloy is an excellent cast magnesium alloy with high specific strength and strong corrosion resistance. It is mainly used in the manufacturing of electrical products. However, the wear resistance of the alloy is poor and a relatively poor wear is a serious hindrance against wider application of AZ91 magnesium alloys. Increasing the wear resistance of this alloy has become one of the important research hotspot.

Changing the microstructure or generating new reinforcements and improving the hardness of the friction surface were the main means for improving the friction properties of AZ91 Mg alloy. The method to improves surface hardness only develops the local anti-wear property of the material, and once the protective layer is damaged, performance is reduced. Auezhan Amanov [4] studied the ultrasonic nanocrystalline surface modification (UNSM) process on the tribological properties of AZ91 Mg alloy. The results showed that the UNSM process can increase the surface hardness and improve the tribological properties of the alloy. E. Correa [5] deposited the electroless Ni-B coatings on AZ91 alloy to improve the alloy's wear resistance. The results show that the wear resistances of the coatings were almost two orders of magnitude greater than that of the uncoated substrates. W. Pakieła [6] investigated the microstructure and mechanical properties of surface layer produced during laser surface treatment. The result showed that laser surface treatment can improve the hardness of the alloy.

Increasing the whole body of the material's anti-friction capability is relatively more reliable. One of the common ways to do so is to change the microstructure of the alloy [7]. Modifying the morphology of the microstructure or generating new reinforcing phases can improve the wear resistance of the alloy. The addition of rare earth elements [1,8,9] to the AZ91 alloy matrix or heat treatment [10] are commonly used means. A. Zafari [4] investigated the effect of 1–3 wt.% of lanthanum-base rare earth elements addition on the wear behavior of AZ91 alloy at wear temperatures of 25–250 °C under a normal load of 20 N. The results showed that lanthanum-base rare earth element additions were not improving the wear rate of the alloys at the wear temperature of 25 °C. The alloy containing 3 wt.% exhibited the highest wear resistance when wear temperatures increased to 150–200 °C. X.J. Wang [11] studied the aging behavior of as-cast SiCp/AZ91 Mg matrix composites. The results show that the aging treatment and SiCp particles were effective in improving the mechanical properties of AZ91 magnesium alloy.

β-$Mg_{17}Al_{12}$ phase has a direct effect on the friction properties of AZ91 alloys, especially at high friction temperature. The β-$Mg_{17}Al_{12}$ phase melting point is between 437 and 458 °C. When the worn surface temperature increased, the β-$Mg_{17}Al_{12}$ may melt and the wear resistance decreases. Addition of rare earth can reduce the number of softer and lower melting β-$Mg_{17}Al_{12}$ phase, and change the morphology of β-$Mg_{17}Al_{12}$ phase. It can generate new rare earth reinforced phases, and improve the wear resistance of the matrix alloy. CUI Xiao-peng [12] studied the microstructure and mechanical properties of die-cast AZ91D magnesium alloy by Pr additions. The mass fraction of Pr at around 0.8% is considered to be suitable to obtain the optimal mechanical properties. However, there are relatively few studies on the effect of Pr on the wear properties of AZ91 alloys. With respect to heat treatment, Yan H. [10] analyzed that T6 heat treatment can dissolve $Mg_{17}Al_{12}$ completely and then renew its precipitation. Li N. [13] believed that that T6 heat treatment benefited for the improvement of the wear properties of the alloy. Based on the above reasons, this paper studied the effect of Pr addition and T6 heat treatment on the microstructure and wear properties of AZ91 alloy under different loads.

2. Experimental

2.1. Materials Preparation

Commercial AZ91 magnesium alloy was chosen as the matrix material. The content of Pr in composites was controlled by the added amount of the Mg-20 wt.% Pr master alloy. And this master alloy was composed of pure Mg-80 wt.% and Pr-20 wt.%. The Pr additions were 0.5, 1.0, and 1.5 wt.%. In order to prevent oxidation of magnesium alloys, SF6 and CO_2 gas mixtures were used for protection during melting. The smelting temperature was first set to 700 °C, and the matrix alloy was kept in heating for 10 min after melting. Then, the temperature of the furnace was heated to 850 °C, and Mg-20 wt.% Pr master alloys wrapped with aluminum foil were added. After mixing, the melting alloy was cooled down to 740 °C, and casted into the metal mold with the ingot size of Φ20 mm × 200 mm. The alloy was subjected to solution treatment at 380 °C for 15 h and then cooled with furnace. Those samples that had been solution-treated were aged at 175 °C for up to 22 h, and also cooled with furnace.

2.2. Wear Testing

The dry sliding wear test was carried out using a MMD-1 (Jinan Yihua Tribology Testing Technology Co., Ltd., Jinan, China) pin-on-disc apparatus at room temperature. The wear tests were carried out in a laboratory atmosphere with a relative humidity ranging from 40% to 60%. The wear rates and friction coefficients results were the average value of the three tests. Pin samples were machined into rods of Φ4.5 mm × 11 mm. The disc material was ASTM1045 steel of 45 HRC. Before each test, the pin and disc surfaces were ground with 600, 1200, 1500, and 2000-grit SiC abrasive paper successively, polished, and then cleaned with ethanol. The surface of the samples was polished to a roughness less than 0.1 μm before wear testing.

A constant sliding speed of 100 rpm (0.188 m/s) and sliding time of 15 min were selected for the tests, while three different applied loads (30, 60 and 90 N) were used employing stationary weights. This experiment used the wear rate as a measure of the material's wear resistance. Samples' densities were determined using the Archimedes' principle. All weight loss data were converted to volume loss using the measured densities. Wear rates were estimated by dividing the volume wear loss by the sliding distance. Friction coefficients were the mean values of the kinetic friction coefficients in steady period of wear (after sliding for 3 min).

2.3. Characterization

A Nikon Eclipse MA200 (Nikon Metrology, Inc., Brighton, UK) optical microscope (OM) was used to observe and analyze the microstructure evolution of the samples. Metallographic specimens were taken from the central position of each ingot. The samples that were used for the OM examination were mounted and then polished and etched in an ethanol solution composed of 4 vol. % nitric acid. The micro-hardness was measured using a HVS-1000A Vickers hardness instrument (Laizhou Huayin Testing Instrument Co., Ltd., Laizhou, China). The set load was 300 g and 10 s duration. The worn surfaces were inspected by a VEGA3 TESCAN (TESCAN CHINA, Ltd., Shanghai, China) scanning electron microscope (SEM) equipped with an energy dispersive spectrometer (EDS).

3. Results and Discussion

3.1. Microstructure Evolution

Figure 1 showed optical microstructures of Mg-xPr alloys with different Pr contents. Each phase was determined by comparing the results of the literature [8] and EDS analysis (Figure 2 and Table 1). The as-cast microstructure of AZ91 alloy consisted of α-Mg and β-$Mg_{17}Al_{12}$. The β-$Mg_{17}Al_{12}$ phase is networked or massively distributed along grain boundaries as Figure 1a shown. As can be seen from Figure 1b, when 0.5% Pr was added, the amount of networked β-$Mg_{17}Al_{12}$ phase in the alloy was significantly reduced, and it was mostly in the form of a block. The black needle-like phase in was $Al_{11}Pr_3$ and the black granular polygonal phase is Al_6Mn_6Pr. It could be observed from Figure 1c that the size of the bulk β-$Mg_{17}Al_{12}$ phase was further reduced, and part of the β-$Mg_{17}Al_{12}$ phase was nearly spherical. The number of $Al_{11}Pr_3$ and Al_6Mn_6Pr phases has increased. Figure 1d showed that β-$Mg_{17}Al_{12}$ phase size increased compared to Figure 1c and had a tendency to become network-like. The amount of $Al_{11}Pr_3$ and Al_6Mn_6Pr phases continued to increase. Therefore, Pr was added at 1.0%, the microstructure obtained was optimal.
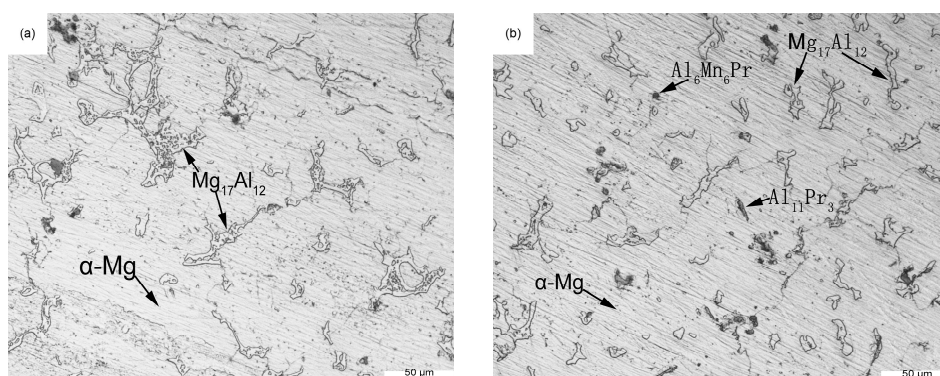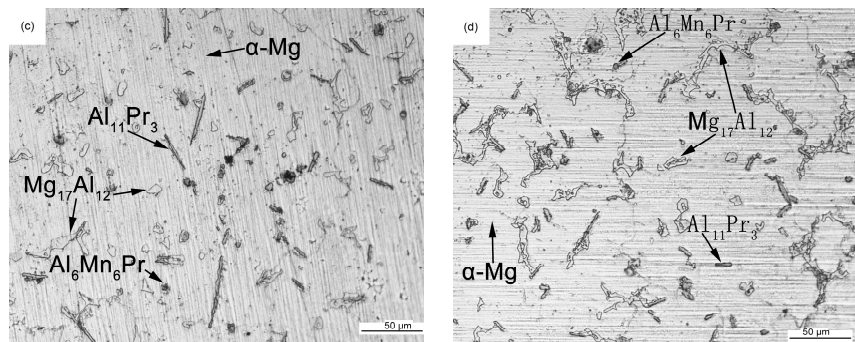

Figure 1. *Cont.*

Figure 1. Optical microstructure of the AZ91-xPr alloys: (**a**) x = 0%, (**b**) x = 0.5%, (**c**) x = 1.0% and (**d**) x = 1.5%.

The three roles of rare earth Pr were:

(1)   Changing the microstructure of the β-$Mg_{17}Al_{12}$ phase;
(2)   Refining the grain size;
(3)   Forming $Al_{11}Pr_3$ and Al_6Mn_6Pr phases, thereby reducing the β-$Mg_{17}Al_{12}$ phase amount.

By addition of the Pr elements, a lower amount of aluminum could become available for the formation of β phase and, subsequently, leading to a change in the morphology of this phase. It can be seen from Figure 3 that the dispersion of the rare earth Pr in the AZ91 magnesium alloy was relatively homogeneous.
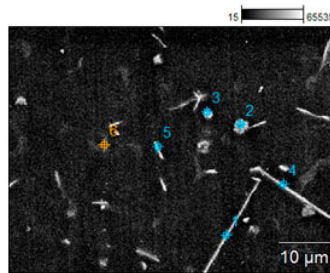
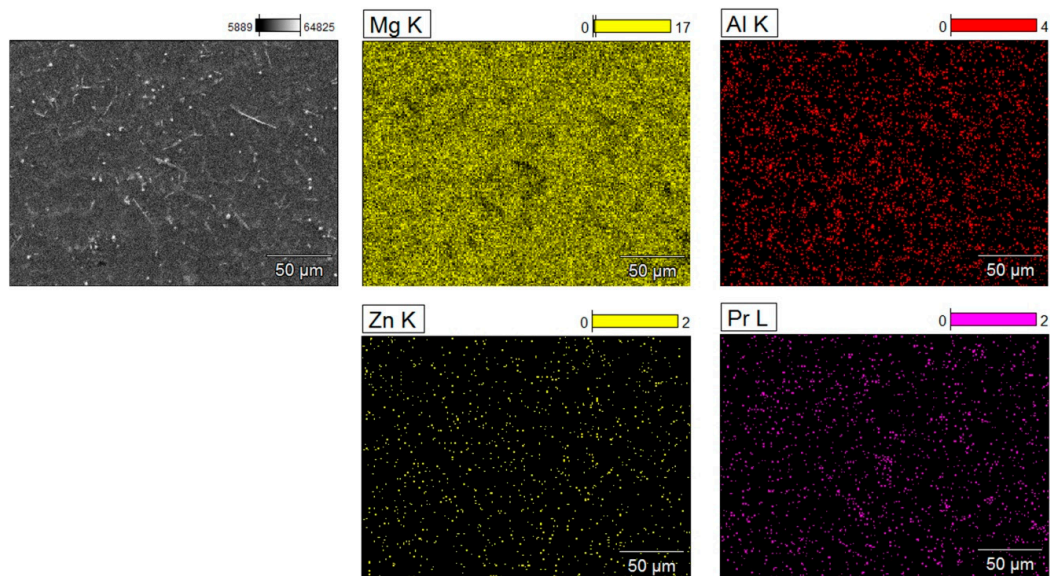**Figure 2.** SEM images of AZ91-1.0%Pr die-casting alloys.

Figure 3. X-ray elemental map of Mg, Al, Zn and Pr of the surface of AZ91-1.0%Pr alloy.

Table 1. EDS analysis results of points in Figure 2.

Point	Weight/%			
	Mg	**Al**	**Mn**	**Pr**
1	70.67	-	0.32	6.27
2	8.86	34.56	24.79	18.47
3	22.31	29.16	20.13	15.37
4	74.45	9.22	-	7.89
5	54.53	27.12	-	10.54
6	62.89	30.01	-	0.21

After solution treatment of the AZ91-1.0%Pr alloy, the original β-$Mg_{17}Al_{12}$ phase dissolved into the α-phase matrix and forms a solid solution, as shown in Figure 4. The Al element distribution tended to be uniform. Fine β precipitates can be seen in the grains. While the needle-like and polygonal granular rare earth phases have a high melting point, their morphology had not changed. After aging treatment as Figure 5 shown, the β phase precipitated out in grains and grain boundary again. The precipitates distributed uniformly in both matrix and grain boundaries after aging [14]. The β precipitations in the grain boundary was in the form of alternating layers, and nearly spherical in the grains.
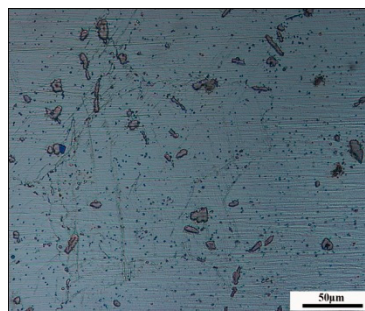
Figure 4. Optical micrographs of AZ91-1.0%Pr alloy after solution treated.
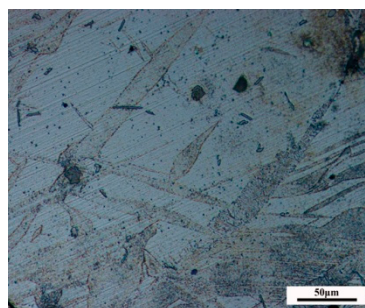
Figure 5. Optical micrographs of AZ91-1.0%Pr alloy after T6 heat treatment.

3.2. Hardness

The hardness results were shown in Figure 6. From the results, it can be seen that with the increase of Pr content, the hardness increased first and then decreased. When the Pr content was 1.0%, the hardness value was the highest and its value was 76.2 HB. The AZ91-1.0%Pr alloy was treated by T6 heat treatment. After solution treatment, the hardness of the alloy decreased and its value was 68 HB. After aging treatment, the hardness of the alloy reached the highest and its value was 101.1 HB. Hardness has a certain effect on the wear properties of the alloy. According to the Archard's law [15], the higher hardness can improve the wear resistance of the alloy. However, there are many factors

that affect wear properties of the alloy. H.C. Meng [16] analyzed the friction models proposed in numerous literatures. He believed that it was not possible to use a single model to accurately predict the wear properties of materials, and there were many factors affecting the wear properties: there were approximately 100 variables or parameters. Therefore, the wear properties cannot be judged from the hardness values alone.
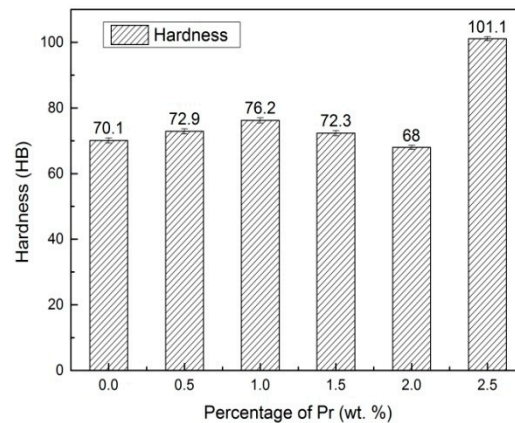

Figure 6. Effect of Pr content on the hardness of alloys.

3.3. Wear Rates

The variation of wear rate by wear testing under normal loads of 30, 60 and 90 N was illustrated in Figure 7. As could be seen from Figure 7, under the same wear conditions, the matrix alloy wear rates were the largest. Adding rare earth element Pr improved the wear resistance of the matrix. With the addition of Pr, the microstructure was refined, the strength of the substrate was enhanced, and the wear properties of the alloy were improved. In the smelting process, rare earth Pr elements reduced casting defects and improved casting quality. Meanwhile, it also purified the grain boundary and increased the grain boundary strength, so it was beneficial to improve the wear resistance of the alloy. The minimum wear rate value appeared at Pr content of 1% and load of 30 N; the maximum ware rate value appeared at Pr content of 0% and load of 90 N. When at the same Pr content, the wear rates increased as the applied load was increased. The wear rate increased slightly when the load increased from 60 N to 90 N. Increasing the load caused the temperature of the grinding surface to rise and the oxide layer increased [17]. An increase in the oxide layer led to a decrease in adhesion, resulting in an increase in the wear rate. However, the oxide layer reduced the contact area of the grinding surface. So, the wear rates increased. In addition, when the load increased, plastic deformation occurred on the worn surface, so that the oxide layer is not easy to adhere on the worn surface [1]. When the load was further increased, the wear rate increased slightly.

The addition of Pr changed the formation and distribution of β-$Mg_{17}Al_{12}$ phase. When the grinding surface temperature rose, the β-$Mg_{17}Al_{12}$ phase lost its strength. Plastic deformation occurred on the grinding surface, and plastic deformation caused the oxide layer cannot adhere to the wear surface. So, under the same wear conditions, the wear rate is the highest when the Pr content was 0%, and the wear rate was the lowest when the Pr content was 1%.
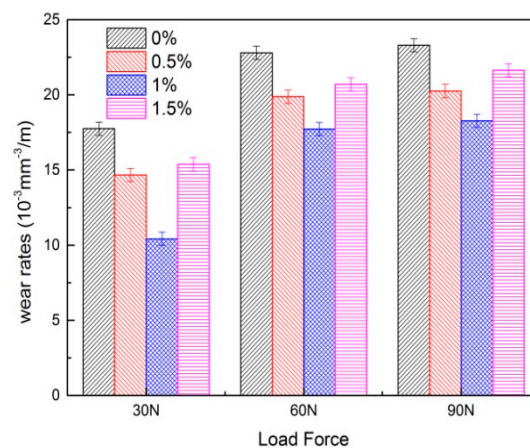
Figure 7. Wear rates of the tested alloy under different load force.

The β phase is the main strengthening phase in AZ91 magnesium alloy. Increase in β phase creates more surfaces for easy deformation and sliding due to the low thermal stability and softening of β phase [8]. The discontinuous and net-shape β phase which distributed along the grain boundary was changed into fine and homogeneous mass shape with the Pr addition, as Figure 1c shown. The existence of thermally stable $Al_{11}Pr_3$ intermetallic compound with high melting point could also help to resist the applied stresses in the contact zones. The higher strength and stability of $Al_{11}Pr_3$ intermetallic compound could make the matrix more stable and improve the wear resistance of the alloy.

The wear rate of the AZ91-1.0%Pr specimens after solid solution and aging treatment compared with the as-cast specimens was shown in Figure 8. Compared with the as-cast, the wear rate of the sample after solution treatment obviously increased, while the wear rate of the sample after T6 decreased. The hardness of the alloy after solution treatment decreased and the wear resistance property decreased. After T6 heat treatment, the hardness of the alloy was increased, and the re-precipitated β phase reduced the stress concentration and enhanced the bonding at particle-to-matrix interface [10].
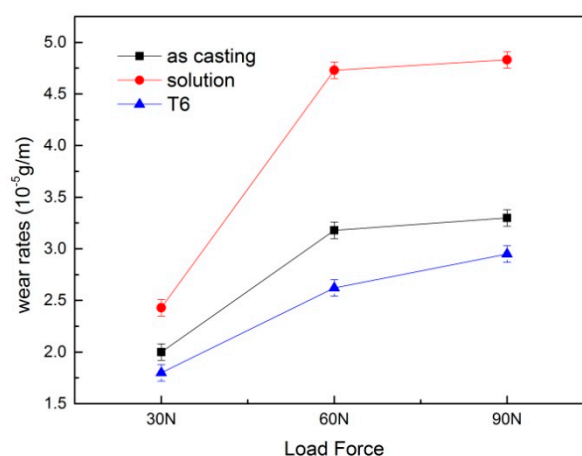

Figure 8. The wear rates of AZ91-1.0Pr as-cast and after heat treatment.

3.4. Friction Coefficient

When the Pr content was the same, the friction coefficient increased as the load increased. The load was to affect the wear property by changing the size of the actual contact area and the degree of plastic deformation on the worn surface. When the load increased, a certain plastic deformation occurred on the worn surface of the original undulations, which increased the actual contact area of the friction pair, resulting in an increase in the friction coefficient. On the other hand, due to the plastic deformation,

the oxide debris cannot be adhered to the worn surface, and the oxide wear debris helps to reduce the friction coefficient. Therefore, the load increased, and the friction coefficient increased due to the detachment of the oxide wear debris.

Under the same friction conditions, when the Pr content was 1%, the friction coefficient was the smallest, and when the Pr content was 0%, the friction coefficient was the biggest (as Figure 9 shown). The rare earth Pr element increased the grain boundary strength and increased the hardness of the alloy, so it was beneficial to improve the wear resistance of the alloy. After adding Pr, the solid solution strengthening effect of the generated $Al_{11}Pr_3$ and Al_6Mn_6Pr phases in the magnesium alloy improved the hardness and yield strength of the AZ91 magnesium alloy. The friction coefficient was related with the microstructure or mechanical properties of the material [18]. And with the increase of Pr content, the hardness increased, and the hardness reached the maximum when Pr content was 1.0%. This improved the wear resistance of the alloy and reduces the friction coefficient. The friction coefficient was the lowest when the hardness was the highest at the Pr content of 1.0%.
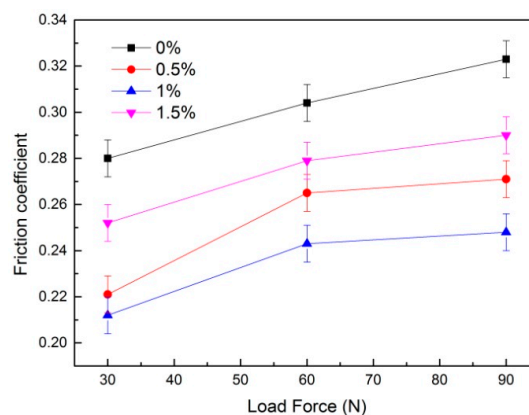

Figure 9. Friction coefficients of the tested alloys under different applied loads.

After solution treatment of AZ91-1.0%Pr alloy, the hardness of the alloy decreased and the plasticity increased. The alloy was more likely to undergo plastic deformation that increased the frictional contact area and increased the friction coefficient. Compared with the friction coefficient of the as-cast, at 30 N, the friction coefficient after the solution treatment of the alloy increases was not obvious, while at 60 N and 90 N, the plastic deformation is more serious, so the friction coefficient increased more obviously, as shown in Figure 10. After T6 heat treatment, β-phase was re-precipitated, which increased the hardness and yield Strength of the alloy [10]. That improved the ability of the alloy to resist deformation. Therefore, after T6 treatment, the friction coefficient decreased.
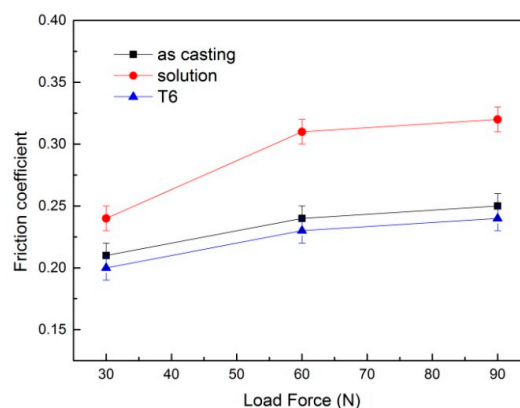

Figure 10. The friction coefficients of AZ91-1.0%Pr as-cast and after heat treatment.

3.5. Wear Mechanisms

Figure 11a showed the worn surface of AZ91-0%Pr alloy under the load of 30 N. The grinding surface was undulated and the wear debris accumulated on the worn surface. The main wear mechanisms were abrasion [19] and oxidation at this condition. The worn surface of AZ91-0%Pr alloy under a load of 60 N was shown as Figure 11b. There were some ploughs with different depth along the wear direction and grooves on the worn surface. Therefore, the main wear mechanisms of this condition were abrasive [20] and delamination. The worn surface of AZ91-0%Pr alloy under a load of 90 N was shown as Figure 11c. In addition to the grooves, a bright band appeared on the worn surface. It indicated that the wear surface undergone plastic deformation. So, the main wear mechanisms were delamination and plastic deformation [10]. The wear resistance of the AZ91-0%Pr alloy decreased as the load increased. The voids can be observed in Figure 11a–c), which was the main feature of the wear of the delamination [21]. Delamination occurred under all tested wear conditions at the Pr content was 0%.
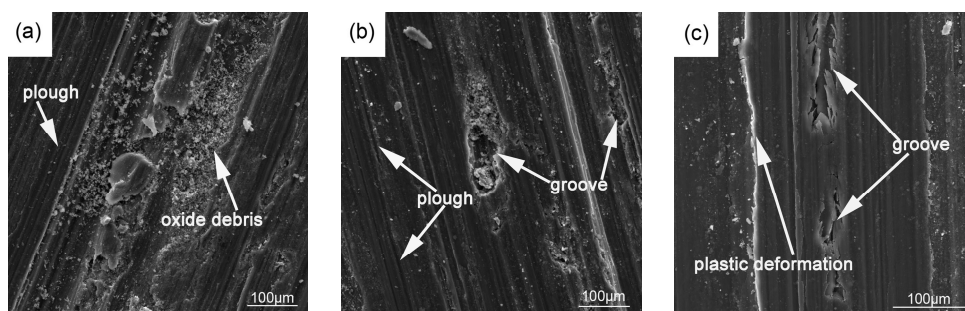

Figure 11. SEM images of worn surface for AZ91-0%Pr alloy under different applied loads (**a**) 30 N, (**b**) 60 N and (**c**) 90 N.

Figure 12a showed the worn surface of AZ91-0.5%Pr alloy under a load of 30 N. There were more abrasive particles on the worn surface. Meanwhile, plough appeared and tear can be observed in the local plough region. At this condition, the main wear mechanisms were abrasion and delamination. Figure 12b showed the worn surface of AZ91-0.5%Pr alloy under a load of 60 N. A large number of scratches were distributed on the wear surface, and a large area of shedding was observed so that a large amount of particles and flakes were formed on the surface. The wear debris, as can be seen from Figure 13, the main components of wear debris on the worn surface were oxygen, magnesium and iron (from the friction disc). The main wear mechanisms at this condition were delamination and oxidation [22]. Figure 12c showed the worn surface of AZ91-0.5%Pr alloy under a load of 90 N. It can be seen that there were widened grooves, localized plastic deformation and larger broken area on the worn surface. The main wear mechanisms were plastic deformation and delamination.
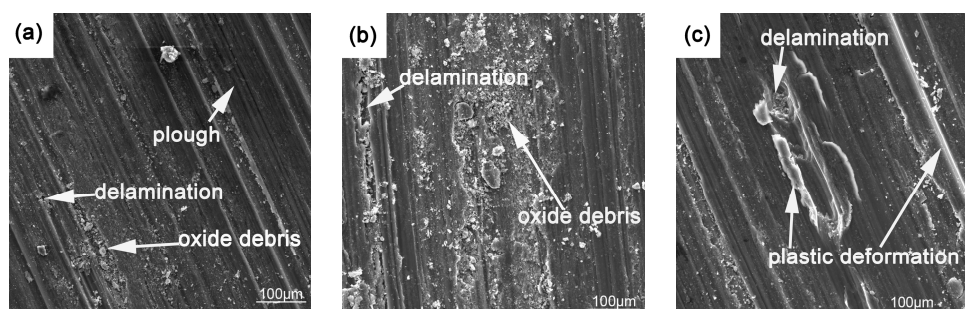

Figure 12. SEM images of worn surface for AZ91-0.5%Pr alloy under different applied loads (**a**) 30 N, (**b**) 60 N and (**c**) 90 N.
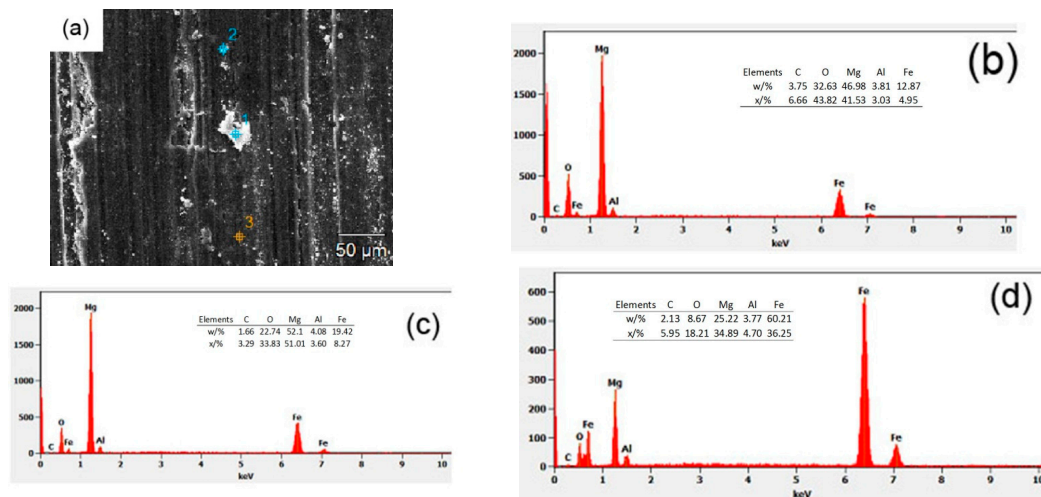
Figure 13. EDS analysis of wear debris (**a**) Location of points, (**b**) point 1, (**c**) point 2 and (**d**) point 3.

Figure 14a shows the worn surface of AZ91D-1.0%Pr alloy under a load of 30 N. Many ploughs with different depths were observed on the worn surface. A large number of oxidized and detached abrasive grains were distributed in the ploughs. The separation of the detached abrasive particles further generated abrasive wear on the surface. Abrasion and oxidation were dominant at this condition, corresponding to mild wear. When the load increased to 60 N, a worn surface was seen (Figure 14b). The wear debris formed on the worn surface due to the detachment of the oxide film, which cut the surface along the direction of wear through the plough, resulted in grooves. A lot of adhesives were flattened on the surface and a small number of cracks were observed. Abrasion and oxidation were dominant at the load of 60 N. When the load increased to 90 N, plastic deformation was observed on the worn surface (as shown in Figure 14c). Due to plastic deformation, oxides could not adhere to the wear surface. There was still a large amount of oxide wear debris in the area with no plastic deformation on the worn surface. Plastic deformation and oxidation were dominant at a load of 90 N.
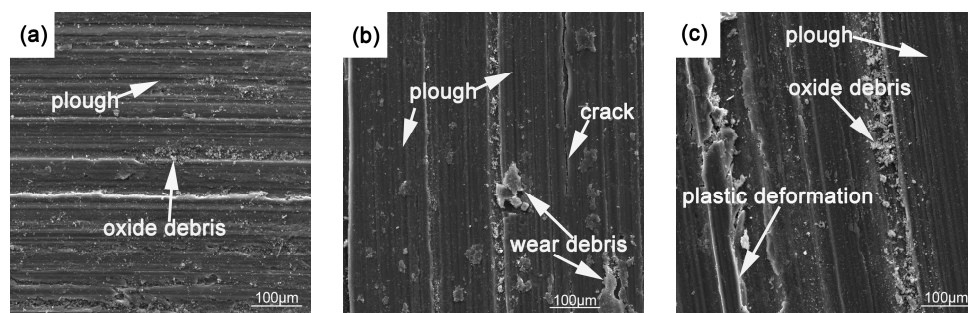

Figure 14. SEM images of worn surface for AZ91-1.0%Pr alloy under different applied loads (**a**) 30 N, (**b**) 60 N and (**c**) 90 N.

Figure 15a–c were the worn surfaces of AZ91-1.5%Pr alloy under the loads of 30 N, 60 N and 90 N, respectively. Under the same conditions, the main wear mechanism was the same as that of AZ91-1.0%Pr alloy. But worn surface became worse.
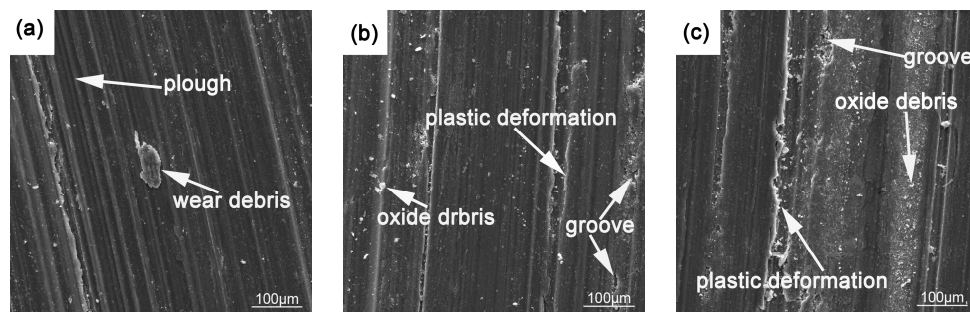
Figure 15. SEM images of worn surface for AZ91-1.5%Pr alloy under different applied loads (**a**) 30 N, (**b**) 60 N and (**c**) 90 N.

As the load increased, the worn surface of the contact areas became worse. Under the same wear conditions, when the Pr content was 1%, the depths of the ploughs and grooves were minimal. That indicated that the alloy has high interfacial bonding strength and the best wear resistance.

Figure 16 shows the worn surface of the AZ91D-1.0%Pr alloy after the solution treatment. There were scratches and plastic deformation parallel to the wear direction at loads of 30 N, 60 N, and 90 N. Compared with Figure 14, under the same wear conditions, the alloy had more severe plastic deformation and more grooves after solution treatment. This indicated that the alloy became soft and wear resistance reduced.
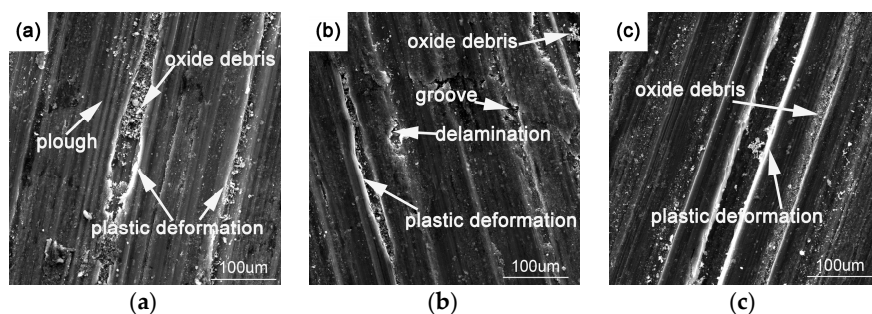

Figure 16. the worn surface of AZ91-1.0%Pr alloys with solution heat treatment under different loads (**a**) 30 N, (**b**) 60 N, (**c**) 90 N.

Figure 17 showed the worn surface of the AZ91-1.0%Pr alloy after T6 treatment. Compared with Figure 14, under the same wear conditions, there were fewer scratches and the wear resistance improved. Abrasion and oxidation were dominant at load of 30 N, corresponding to mild wear [22]. Simultaneously, delamination and plastic deformation were mainly at high loads of 60 N and 90 N, which related to severe wear.
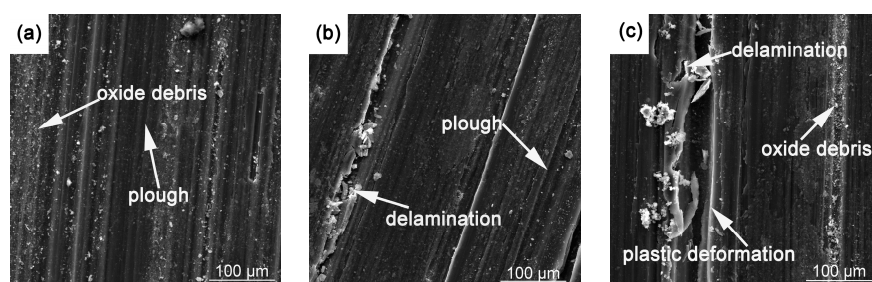

Figure 17. the worn surface of AZ91-1.0%Pr alloys with T6 heat treatment under different loads (**a**) 30 N; (**b**) 60 N; (**c**) 90 N.

4. Conclusions

This paper investigated the influence of Pr addition and heat treatment (T6) on the dry sliding wear behavior of AZ91 alloy by pin-on-disc tribometer. The conclusions of this investigation wereas follows:

(1) Rare earth Pr refines the microstructure of AZ91 alloy and generates new reinforcing phase. When the Pr content is 1%, the refinement effect is best, and its hardness reaches a peak value of 76.2 HB. After the T6 heat treatment of AZ91-1.0%Pr alloy, the β phase precipitated out in grains and grain boundary again. The β precipitations in the grain boundary was in the form of alternating layers, and nearly spherical in the grains. Meanwhile, the hardness of the alloy is further increased to 101.1 HB, which is a 45% increase in hardness compared to the AZ91 as-cast alloy.

(2) As the load increases, the wear rate and friction coefficient all increased. The AZ91-1.0%Pr alloy with T6 exhibited both the lowest wear rates and friction coefficients of all the alloys. The AZ91-1.0%Pr alloy treated with T6 treatment showed better wear resistance, which was mainly due to large amounts of fine $Mg_{17}Al_{12}$ distributed in the grains and grain boundary. After T6 heat treatment, the wear rate was reduced by approximately 50% compared to the as-cast alloy at 60 and 90 N loads.

(3) As the load increases, the worn surface becomes worse. Abrasive was dominant at load of 30 N, delamination was dominant at load of 60 N and plastic deformation was dominant at load of 90 N. Oxidation was observed at all loads. Abrasion and oxidation were corresponding to mild wear, delamination and plastic deformation were related to severe wear.

The result showed that the addition of Pr or T6 heat treatment is an effective method to improve the wear resistance of AZ91 alloy. This provides valuable information for the preparation of wear-resistant components for electric vehicles. Meanwhile, it also provides a way for reducing the frictional resistance of magnesium alloys during the extrusion, rolling, forging and other processes.

Author Contributions: L.N. and Y.H. conceived and designed the experiments; L.N. performed the experiments; L.N. and Y.H. analyzed the data; L.N. and Y.H. contributed reagents/materials/analysis tools; L.N. and Y.H. wrote the paper.

Conflicts of Interest: The author declares no conflict of interest.

References

1. Zafari, A.; Ghasemi, H.M.; Mahmudi, R. An investigation on the tribological behavior of AZ91 and AZ91+3 wt% RE magnesium alloys at elevated temperatures. *Mater. Des.* **2014**, *54*, 544–552. [CrossRef]
2. Pan, F.s.; Yang, M.B.; Chen, X.H. A Review on Casting Magnesium Alloys: Modification of Commercial Alloys and Development of New Alloys. *J. Mater. Sci. Technol.* **2016**, *32*, 1211–1221. [CrossRef]
3. García-Rodríguez, S.; Torres, B.; Maroto, A. Dry sliding wear behavior of globular AZ91 magnesium alloy and AZ91/SiCp composites. *Wear* **2017**, *390–391*, 1–10. [CrossRef]
4. Amanov, A.; Penkov, O.V.; Pyun, Y.S. Effects of ultrasonic nanocrystalline surface modification on the tribological properties of AZ91D magnesium alloy. *Tribol. Int.* **2012**, *54*, 106–113. [CrossRef]
5. Correa, E.; Zuleta, A.A.; Guerra, L. Tribological behavior of electroless Ni–B coatings on magnesium and AZ91D alloy. *Wear* **2013**, *305*, 115–123. [CrossRef]
6. Pakiela, W.; Tanski, T.; Brytan, Z.; Labisz, K. The influence of laser alloying on the structure and mechanical properties of AlMg5Si2Mn surface layers. *Appl. Phys. A-Mater.* **2016**, *122*, 352. [CrossRef]
7. Snopiński, P.; Tański, T.; Labisz, K.; Rusz, S.; Jonsta, P. Wrought aluminium–magnesium alloys subjected to SPD processing. *Int. J. Mater. Res.* **2016**, *107*, 637–645. [CrossRef]
8. Zafari, A.; Ghasemi, H.M.; Mahmudi, R. Effect of rare earth elements addition on the tribological behavior of AZ91D magnesium alloy at elevated temperatures. *Wear* **2013**, *303*, 98–108. [CrossRef]

9.   Asl, K.M.; Masoudi, A.; Khomamizadeh, F. The effect of different rare earth elements content on microstructure, mechanical and wear behavior of Mg–Al–Zn alloy. *Mater. Sci. Eng. A* **2010**, *527*, 2027–2035.

10.   Yan, H.; Wang, Z.W. Effect of heat treatment on wear properties of extruded AZ91 alloy treated with yttrium. *J. Rare Earth* **2016**, *34*, 308–314. [CrossRef]

11.   Wang, X.J.; Hu, X.S.; Liu, W.Q.; Wu, K.; Huang, Y.D.; Zheng, M. Ageing behavior of as-cast SiCp/AZ91 Mg matrix composites. *Mater. Sci. Eng. A* **2017**, *682*, 491–500. [CrossRef]

12.   Cui, X.P.; Liu, H.F.; Meng, J.; Zhang, D.P. Microstructure and mechanical properties of die-cast AZ91D magnesium alloy by Pr additions. *Trans. Nonferrous Met. Soc. China* **2010**, *20*, 435–438. [CrossRef]

13.   Li, N.; Yan, H.; Wang, Z.W. Effects of Heat Treatment on the Tribological Properties of Sicp/Al-5Si-1Cu-0.5Mg Composite Processed by Electromagnetic Stirring Method. *Appl. Sci. Basel* **2018**, *8*, 372. [CrossRef]

14.   Mthirumurugan, M.; Kumaran, S. Extrusion and precipitation hardening behavior of AZ91 magnesium alloy. *Trans. Nonferrous Met. Soc. China* **2013**, *23*, 1595–1601. [CrossRef]

15.   Archard, J.F. Contact and rubbing of flat surfaces. *J. Appl. Phys.* **1953**, *24*, 981–988. [CrossRef]

16.   Meng, H.C.; Ludema, K.C. Wear models and predictive equations: their form and content. *Wear* **1995**, *44*, 181–183. [CrossRef]

17.   Zafari, A.; Ghasemi, H.M.; Mahmudi, R. Tribological behavior of AZ91D magnesium alloy at elevated temperatures. *Wear* **2012**, *292–293*, 33–40. [CrossRef]

18.   An, J.; Li, R.G.; Lu, Y.; Chen, C.M.; Xu, Y.; Chen, X.; Wang, L.M. Dry sliding wear behavior of magnesium alloys. *Wear* **2008**, *265*, 97–104. [CrossRef]

19.   Aung, N.N.; Zhou, W.; Lim, L.E.N. Wear behaviour of AZ91D alloy at low sliding speeds. *Wear* **2008**, *265*, 780–786. [CrossRef]

20.   Li, P.; Lei, M.K.; Zhu, X.P. Dry sliding tribological behavior of AZ31 magnesium alloy irradiated by high-intensity pulsed ion beam. *Appl. Surf. Sci.* **2010**, *257*, 72–81. [CrossRef]

21.   Mert, F. Wear behaviour of hot rolled AZ31B magnesium alloy as candidate for biodegradable implant material. *Trans. Nonferrous Met. Soc. China* **2017**, *27*, 2598–2606. [CrossRef]

22.   Chen, H.; Alphs, A.T. Sliding wear map for the magnesium alloy Mg-9Al-0.9Zn (AZ91). *Wear* **2000**, *246*, 106–116. [CrossRef]